International Journal of Multiphase Flow 36 (2010) 166–183

Contents lists available at ScienceDirect

International Journal of Multiphase Flow

journal homepage: www.elsevier.com/locate/ijmulflow

Nonlinear dynamic analysis of large diameter inclined oil–water two phase flow pattern

Yan-Bo Zong, Ning-De Jin *, Zhen-Ya Wang, Zhong-Ke Gao, Chun Wang

School of Electrical Engineering and Automation, Tianjin University, Tianjin 300072, China

ARTICLE INFO

Article history:
Received 12 March 2009
Received in revised form 21 September 2009
Accepted 1 November 2009
Available online 14 November 2009

Keywords:
Inclined oil–water flows
Flow pattern dynamics
Conductance probe
Recurrence quantification analysis
Attractor geometric morphology

ABSTRACT

We experimentally investigate the inclined oil–water two phase flow characteristics in 125 mm inner diameter pipe by using the vertical multi-electrode array (VMEA) conductance probe and mini-conductance probes. For the oil and water superficial velocities in the range of 0.0052–0.3306 m/s and inclination angle at 15° and 45° from vertical, we observe the four typical inclined oil–water flow patterns, i.e., Dispersion of oil-in-water-Pseudoslugs, Dispersion oil-in-water-Countercurrent, Transitional Flow and Dispersion of water-in-oil flow pattern. Since the mini-conductance probes are sensitive to local change of flow pattern, with the help of high speed camera, we exactly identify different flow patterns under different flow conditions by analyzing the measured signals. In addition, we also propose the inclined oil–water two phase flow pattern maps for large diameter pipe. Furthermore, we further characterize the flow patterns by applying recurrence quantification analysis and chaotic attractor geometry morphological description to VMEA signals. The results show that the proposed nonlinear analysis method is an effective tool not only for classifying different water-dominated flow patterns but also for characterizing the complex flow structure of inclined oil–water two phase flow system.

1. Introduction

Inclined oil–water flows are common phenomena in petroleum industry, such as oil wells and crude oil transportation system. During the oilfield development, production logging interpretation model often needs flow pattern information, and pressure drop prediction in inclined oil wells also strongly depend on flow behavior. Due to many complex factors, such as gravity, fluid turbulence, the interaction and local relative motion between phases, etc., the inclined oil–water flow presents high irregularity and instability. Especially at large inclination angles from vertical, the intermittent growing or attenuating internal waves (Kelvin–Helmholtz Wave) will happen, the wave structure, local velocity and phase fraction in radius direction are so complex that it is difficult to describe the details of flow structure even in using the computational fluid dynamics technique. So far, inclined oil–water flow pattern transition mechanism is still an unsolved problem.

In early studies, semi-empirical and semi-theoretical methods were often employed in the study of inclined oil–water two phase flows. Mukherjee et al. (1981) studied the effect of input liquid fraction and inclination angles on water holdup and friction pressure gradient in 38.1 mm ID pipe with inclination angels from ±30 to ±90°, and found that the maximum friction pressure gradient at phase inversion point and oil–water slippage are both functions of inclination angles. In 152 mm ID pipe, Hill and Oolman (1982) found that the most troublesome effect of well deviation on production logging tool response is the non-uniform phase distribution across the pipe section. They observed a kind of segregated flow pattern with water phase occupying most of the pipe and steady reverse flow of water along the bottom pipe, and indicated that little change of deviation angels will cause great change of velocity profile distribution. Davarzani et al. (1985) observed two type of flow patterns in a 160 mm ID pipe at inclined 30°, which are stratified flow and stratified wavy flow respectively. Zavareh et al. (1988) concluded that countercurrent bubble flow pattern exists over a wide range of flow conditions in 184 mm ID pipe at inclined 5° and 15°, and described the characteristics of countercurrent bubble flow and dispersed bubble flow patterns. Vigneaux et al. (1988) measured the inclined oil–water flows in 200 mm ID pipe by using high frequency impedance probe, and summarized two main flow patterns of dispersed oil-in-water-pseudoslugs flow and dispersed oil-in-water-countercurrent flow. Tabeling et al. (1991) found that mean holdup and deviation angle are main parameters controlling mean flow structure, while total flow rate has little effect on the overall shape of velocity profiles. Based on "equivalent mixing layer" idea, they also proposed a phenomenological model for local phase holdup. Ding et al. (1994) tested that the modified drift flux model is useful for water holdup prediction in vertical and deviated oil–water flow systems. Hasan and Kabir (1998) concluded that the drift flux of oil phase depends

* Corresponding author. Tel./fax: +86 22 27407641.
E-mail address: ndjin@tju.edu.cn (N.-D. Jin).

0301-9322/$ - see front matter © 2009 Elsevier Ltd. All rights reserved.
doi:10.1016/j.ijmultiphaseflow.2009.11.006

on its in situ volume fraction in addition to the terminal bubble rise velocity in vertical and deviated oil–water flows. It is worth to point out that Flores et al. (1999) made a comprehensive experimental study in vertical and inclined oil–water flows with 50.8 mm ID pipe. They summarized seven flow patterns in inclined oil–water flows with four water-dominated, two oil-dominated and a transitional flow pattern (TF). The water-dominated flow patterns include Dispersion of oil-in-water-Pseudoslugs (D O/W PS), Dispersion of oil-in-water-Countercurrent (D O/W CT), Dispersion of oil-in-water-Cocurrent (CC) and Very fine dispersion of oil-in-water (VFD O/W). The oil-dominated flow patterns are Dispersion of water-in-oil (D W/O) and Very fine dispersion of water-in-oil (VFD W/O). Lucas and Jin (2001a,b) studied the drift velocity model in inclined oil-in-water pipe flows, and indicated that the phase distribution parameter and single droplet terminal rise velocity are greatly affected by inclination angles. By using resistance cross-correlation flow meter, they also found that the measured property of cross-correlation velocity depends on flow patterns, especially at 60°. Dong et al. (2001) discussed the applicability of flow pattern identification by using the electrical resistance tomography technique in inclined and horizontal pipes. Oddie et al. (2003) investigated gas–water, oil–water and oil–gas–water multiphase flows in 150 mm ID inclinable pipe by using several water holdup measurement techniques, and three type of flow patterns are identified at inclination angles less than 70°, which are Semi-mixed flow, Dispersed flow and Homogeneous flow pattern. Lum et al. (2006) experimentally studied the pipe inclination effect on flow pattern, holdup and pressure gradient in 38 mm ID stainless steel pipe, and they found that oil plug flow pattern exists at 80° and 85°, the stratified wavy flow pattern will disappear at 95°.

Since the 1990s, numerical simulation methods have been widely used in the study of inclined oil–water flows. Mobbs and Lucas (1993) proposed a turbulent model of large amplitude Kelvin–Helmholtz eddy qualitative characteristics for inclined liquid–liquid flow, and indicated that the eddy will periodically grow and eclipse, and the largest amplitude of which can reach pipe diameter. Lucas (1995) proposed a mathematical model of velocity profile for inclined oil–water flows, the prediction result of local velocity is close to experiments in upper and central part of the pipe, but far from the bottom of the pipe. Brauner (2002) theoretically studied the near horizontal liquid–liquid flows, and indicated that fluid property parameters will remarkably affect flow pattern transition, such as Eotvös number, liquid velocity, the interfacial density difference, surface intension and viscosity. Other researchers have done similar works (Trallero and Brill, 1996; Al-Wahaibi and Angeli, 2007; Al-Wahaibi et al., 2007).

For nonlinear dynamics of inclined oil–water flows, our previous works in Daqing Oilfield multiphase flow loop facility indicated that, based on the conductance fluctuating signals measured from VMEA sensor, the water-dominated and transitional flow pattern could be effectively identified by using the multi-scale recurrence plot analysis method. But because of the indistinct definition of flow pattern in experimental observation, it is difficult to differentiate between D O/W PS and D O/W CT flow pattern. As a consequent research, the purpose of this paper is to further investigate the two water-dominated flow patterns, i.e., D O/W PS and D O/W CT flow, and explore the corresponding nonlinear dynamics by analyzing the signals measured from the mini-conductance probes as well as the VMEA sensor. The flow pattern definition in our experiment is mainly based on the response of mini-conductance probes, and the nonlinear dynamics of flow pattern is characterized by using the recurrence plot (recurrence quantification analysis) and chaotic attractor geometry morphological description. In particular, we propose a new nonlinear analysis method, which is based on the attractor geometry morphological area, long axis and short axis. Finally, we propose the inclined oil–water flow pattern maps at 15° and 45° respectively. The results indicates that the two main water-dominated flow patterns, i.e., D O/W PS and D O/W CT flow, can be effectively identified by using recurrence quantification analysis and chaotic attractor geometry morphological description.

2. Experimental flow loop facility and data acquisition

The experiments of inclined oil–water flows were carried out in multiphase flow laboratory of Tianjin University. The schematic of flow loop facility is shown in Fig. 1. The 125 mm ID transparent Plexiglas pipes is 6 m long and can be inclined at any angle from vertical (0°) to horizontal (90°), the transparent pipe enables visualization of the flow patterns. The flow rates of oil and water phase can be measured by calibrated turbine and electromagnetic flow meter.

Fig. 2 shows the experimental setup of inclined oil–water flows. VMEA and mini-conductance probes are installed at 3 m from the inlet in test section. The structure of VMEA probe is shown in Fig. 3, the details of VMEA probe have been described by Jin et al. (2008). The mini-conductance probes have been widely used for flow pattern identification in gas–water or oil–water flow systems (Flores et al., 1999; Trallero and Brill, 1996; Angeli and Hewitt, 2000; Fairuzov et al., 2000). For the purpose of local parameters measurement, multi-sensor conductance probes were also used by some researchers (Hogsett and Ishii, 1997; Wu and Ishii, 1999; Ishill and Kim, 2001; Hibiki et al., 2003; Lucas and Mishra, 2005). Fig. 4 shows the geometry structure of mini-conductance probes, the outer diameter of conductive casing is 3 mm and it is small enough to avoid changing local flow pattern character, which has been validated by high speed Video Camera Recorder (VCR). For the purpose of flow pattern identification, five mini-conductance probes were arrayed in equidistance at test section, and the distance of each probes in flow direction is 150 mm. Fig. 5 shows the installation schematics of mini-conductance probes, which are inserted at different depth. Probe A, B, C, D, E are respectively at 1/8D, 1/8D, 1/4D, 1/4D, 1/2D from pipe wall, where D = 125 mm is pipe diameter. When the flow loop is inclined from vertical, probe A and C are in the upper part of the pipe, probe E in middle region and probe B and D at the bottom part of the pipe.

The mini-conductance probes are mainly composed by needle electrode and conductive casing, the space between them is filled with insulation. To avoid the polarization of needles, the conductive casing is excited by +5 V and the needle electrodes act as measurement port. In experiments, when the needle electrode was surrounded by conductive water, the circuit formed between needle electrode and casing, the corresponding output signals were at low voltage; when the needle electrode was immerged in non-conductive oil, the circuit was broken, and the corresponding output signals would perform high voltage. The output signals from needle electrode are modulated by a follower circuit and acquired by data acquisition card PXI-4472 and PXI-6115 under the control of LabVIEW software, the analogue to digital converters in PXI-4472 and PXI-6115 card are respectively 24 bits and 12 bits. The modulating circuit of mini-conductance probe is shown in Fig. 6. Influenced by mixed degree of oil and water and fluids velocity, the circuit between needle electrode and the conductive casing usually does not at ideal on–off state, but presents some equivalent resistance character, which is more obvious in water-dominated flow patterns.

The experimental mediums are tap water and No. 15 industry white oil, the oil density is 856 kg/m^3, viscosity is 11.984 mPa s (40 °C) and surface tension is 0.035 N/m. The medium of water phase is dyed with red colored for the convenience of observation, the inclination angles are 15° and 45° from vertical respectively. At each inclination angle, the experimental process is increasing oil flow rates at fixed water flow rates, when both phases flow rates

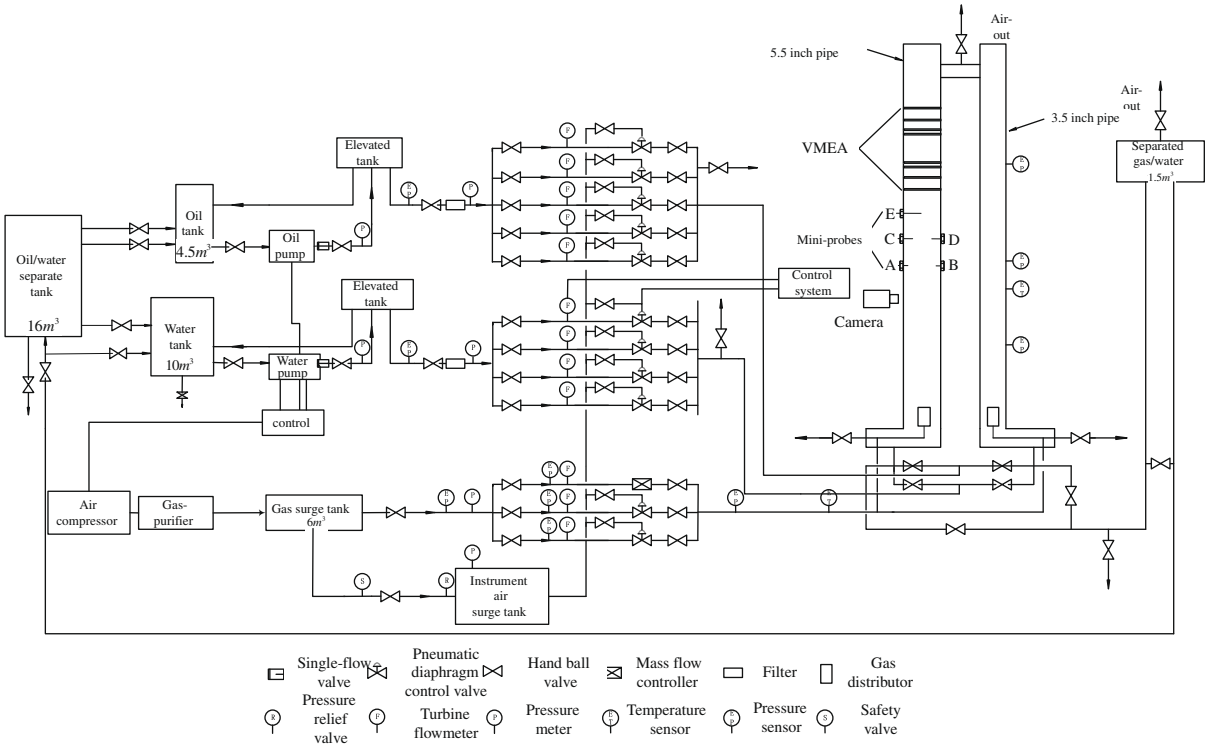

Fig. 1. Schematics of oil/gas/water three phase flow loop facility in Tianjin University.

Fig. 2. Schematics of inclined oil–water two phase flow experiment.

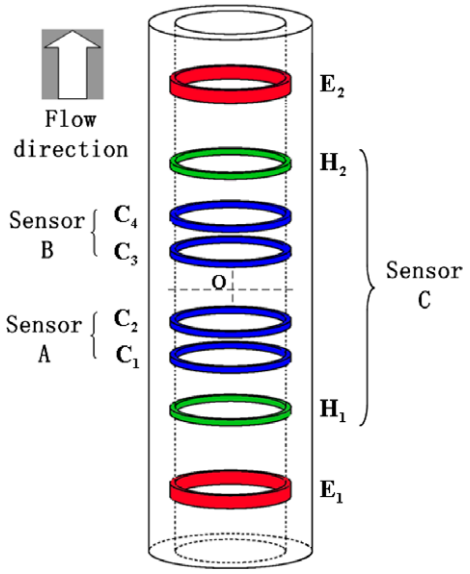

Fig. 3. Structure of VMEA probe.

reach into steady flow condition, the measurement system is started and the flow pattern in each flow conditions is observed and the fluctuating signals of VMEA probe and mini-conductance probe are recorded simultaneously. In experiment, the oil and water superficial velocities are in the range of 0.0052–0.3306 m/s respectively, the sampling frequency of VMEA and mini-conductance probes are 400 Hz, and the duration of sampling is 30 s. More details of data acquisition system can be referenced in our previous publications (Jin et al., 2008; Zheng et al., 2008).

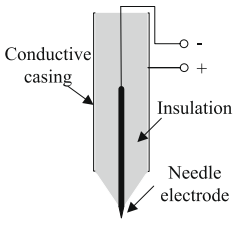

Fig. 4. Structure of mini-conductance probe.

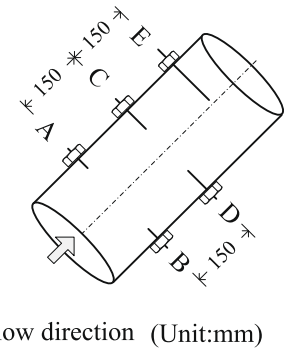

Fig. 5. Installation schematics of mini-conductance array probe.

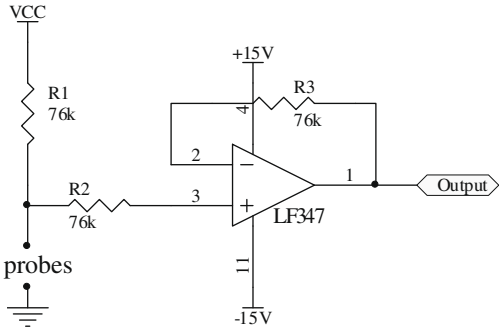

Fig. 6. Conditioning circuit of mini-conductance probe.

3. Experimental results and flow pattern maps

3.1. Flow pattern description based on mini-conductance probes

In inclined oil–water flow conditions, at normal oil and water flow rates, oil phase will gather in the upper side of the pipe, while water phase will present local countercurrent flow in the bottom side of the pipe. Four flow patterns have been observed in this experiment, which are D O/W PS, D O/W CT, TF and D W/O flow pattern respectively. Fig. 7a–d show typical mini-conductance probe signals in different flow patterns with the increasing of oil superficial velocity (U_{so}) at fixed water superficial velocity (U_{sw}) of 0.0374 m/s. The location of each probe has been shown in Fig. 5.

The D O/W PS flow pattern occurs at low to moderate oil and water superficial velocities in large diameter pipe. In this flow pattern, oil phase will form intermittent oil swarms in the upper side of the pipe and move fast in the upward direction, while countercurrent water flow exists at the bottom of the pipe for the effects of pressure, viscosity and gravity component in the opposite direction of main flow. Fig. 7a shows the typical probe signals in D O/W PS flow pattern. In inclined conditions, since probe A is the nearest to the upper side of the pipe wall, probe A signals show much more intermittent positive fluctuations from low to high voltage than others, probe C signals show that a little intermittent positive fluctuations exist in this probe location, while other three probes, i.e., probe B, D and E, almost do not change at low voltage, which indicate that these probes are surrounded completely by water, and all probes present water-dominated flow pattern. By comparing signals of probe A and C, it can be seen that the intermittent oil swarms concentration becomes less and less from the upper side to the lower side of the pipe. In this experiment, the D O/W PS flow pattern occurs in a quite wide range of flow

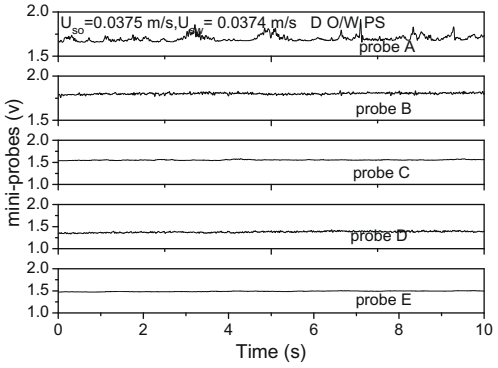

(a) D O/W PS(U_{so}=0.0375 m/s,U_{sw}=0.0374 m/s)

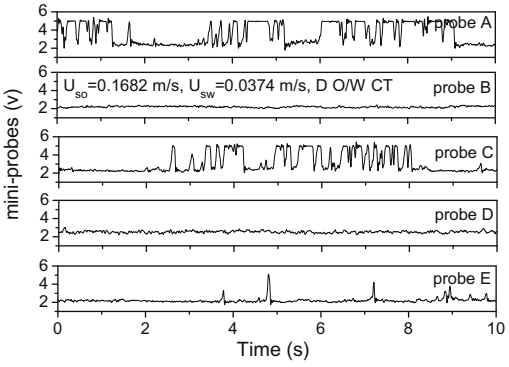

(b) D O/W CT(U_{so}=0.1682 m/s, U_{sw}=0.0374 m/s)

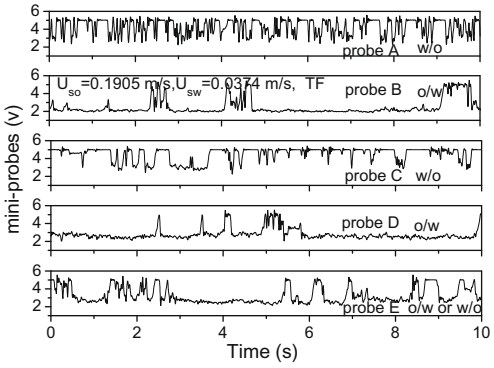

(c) TF (U_{so}=0.1905 m/s,U_{sw}=0.0374 m/s)

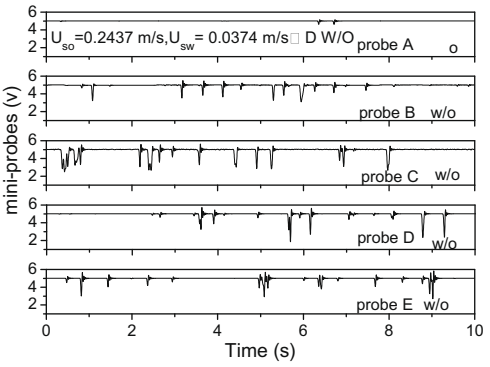

(d) D W/O (U_{so}= 0.2437 m/s,U_{sw}=0.0374 m/s)

Fig. 7. The mini-conductance array probe signals in four typical flow pattern when inclined angle at 45° from vertical.

conditions, which include the whole range of water superficial velocity and most of oil superficial velocity.

The D O/W CT flow pattern occurs at low to moderate water superficial velocities and moderate oil superficial velocities. In D O/W PS flow pattern, increasing oil phase flow rates at fixed water phase flow rates, the interval between oil swarms will become shorter and shorter, and disappear at certain oil phase flow rates at last, at this time, the flow pattern will translate into D O/W CT flow. In this flow pattern, water-countercurrent flow at bottom side of the pipe still exists, which also causes counter flow of some oil droplets far away from the top side of the pipe. Fig. 7b shows the typical probe signals in D O/W CT flow pattern. Probe A shows that local oil-in-water flow and water-in-oil flow pattern alternatively occurs in this flow conditions, this phenomena also occurs in probe C, just more oil-in-water flow and less water-in-oil flow pattern exist in probe C location. Probe E, locating at the central of the pipe, indicates some oil droplets, and presents local oil-in-water flow pattern. Both probe B and D, at the bottom of the pipe,

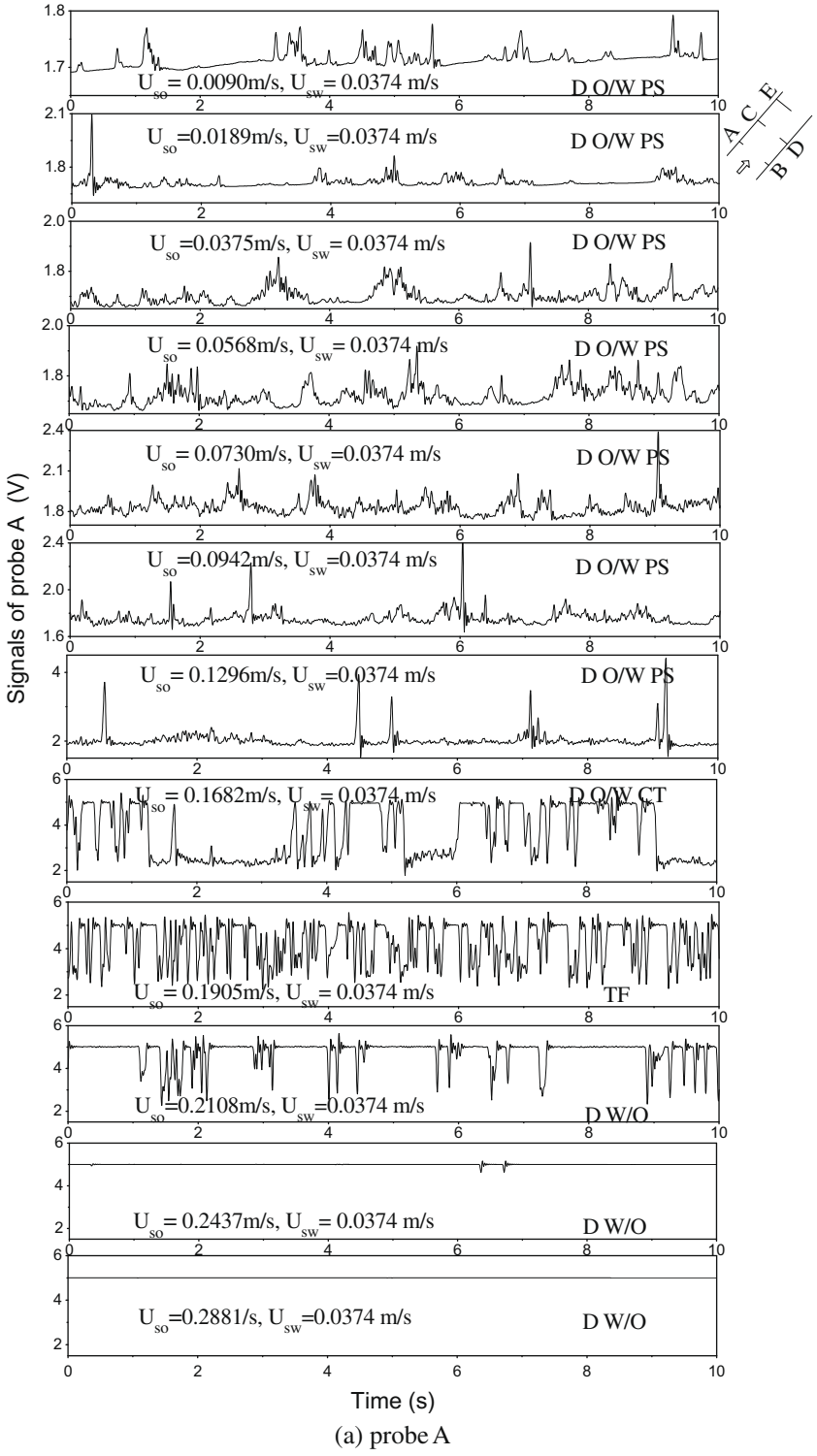

Fig. 8. The mini-conductance probe signals at different flow patterns (inclination 45°, U_{sw} = 0.0374 m/s, U_{so} = 0.0090–0.2881 m/s).

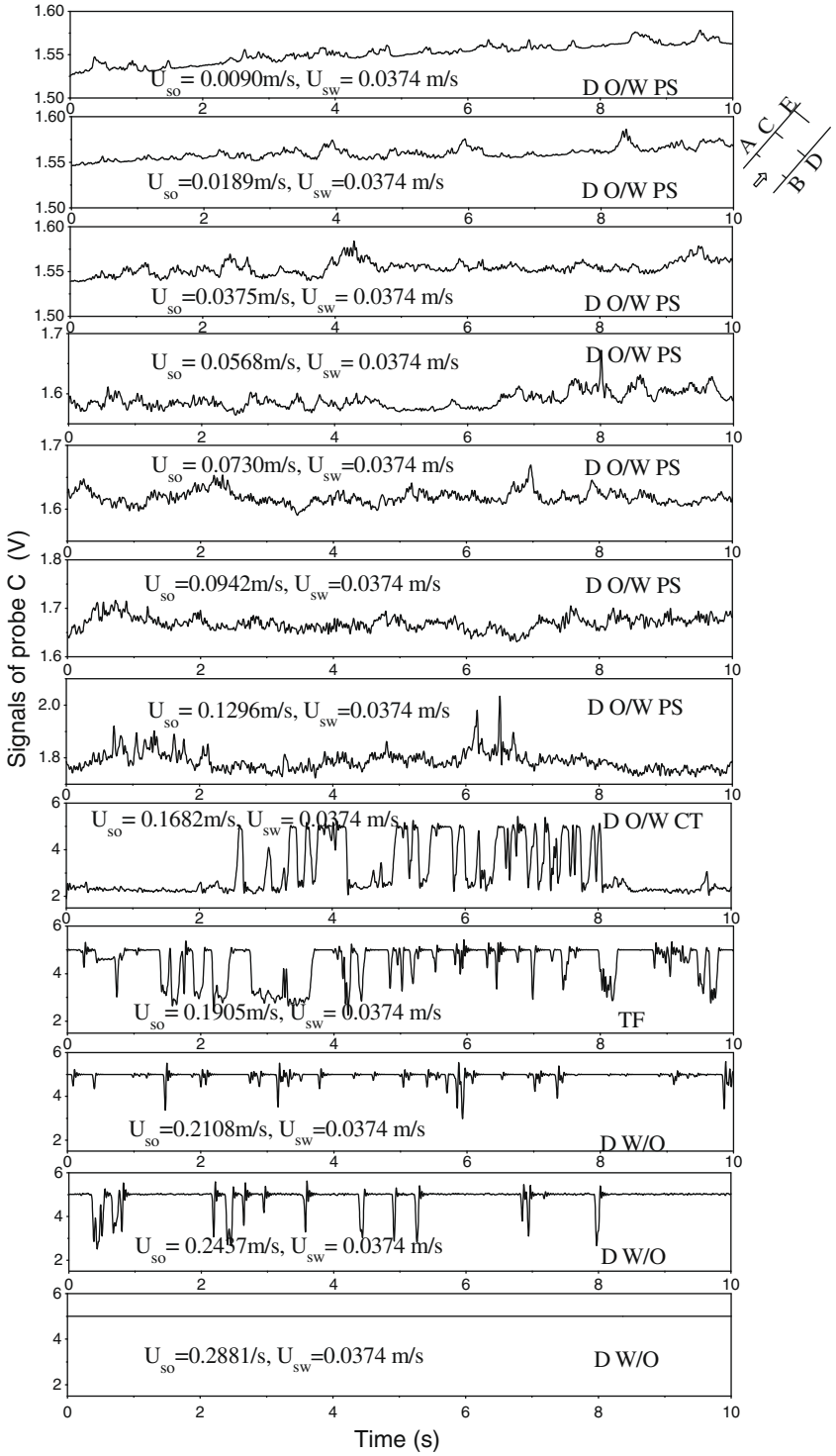

(b) probe C

Fig. 8 (*continued*)

still present low voltage, which is the character of continuous water flow. In this flow pattern, the transitional flow in upper side of the pipe indicated by probe A and C is rarely reported in related literatures. For the flow pattern maps proposed by Flores et al. (1999) in 50.8 mm ID pipe, the D O/W CT flow pattern occurs in wide range of oil and water superficial velocities, while in 125 mm ID pipe, this flow pattern occurs in a quite narrow range of oil and water superficial velocities in this experiment.

The TF flow pattern also occurs in a quite narrow range of oil and water superficial velocities in large diameter pipe. Further increasing oil flow rate in D O/W CT flow, the flow pattern will be translated into the transitional flow (TF). For unsteady transitional flow pattern, oil swarms will coalesce into larger swarms, and for the effects of agglomeration, coalescence and gravity components, thin and elongated oil film will form at the top of the pipe; Below the oil film, oil-dominated and water-dominated flow pattern alternation

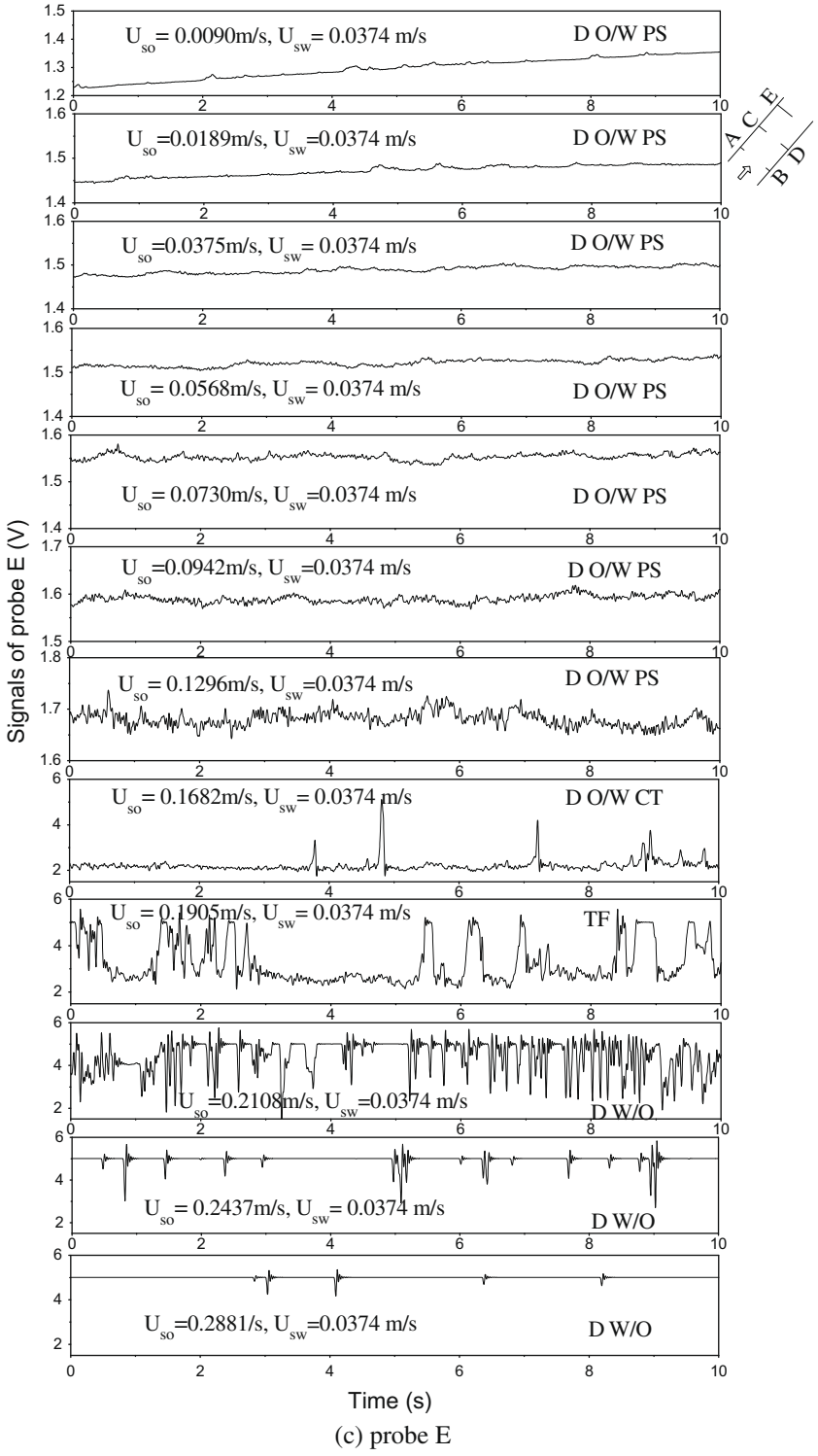

(c) probe E

Fig. 8 (*continued*)

process will occur; local flow pattern at the bottom of the pipe is still oil-in-water flow. Fig. 7c shows the typical probe signals in TF flow pattern. Locating at the upper side of the pipe, probe A and C signals show typical negative pulses from high voltage to low voltage, which is the character of water-in-oil flow pattern. In this flow pattern, probe A and C are mainly surrounded by oil phase, whose signals will always keep high voltage, only when some dispersed water droplets come to touch the probe, the signals will fall down from high to low, and once the water droplets leave the probes, the signals will back to high voltage again. Therefore, probe A presents local water-in-oil flow pattern, and probe C that is further than probe A from the top side of the pipe, mainly presents water-in-oil flow pattern and a little oil-in-water flow pattern once in a way. Probe E, at the middle region of the pipe, shows that oil-in-water flow and water-in-oil flow pattern alternatively occurs, and the local oil-in-water flow pattern is predominant. Probe D indicates continuous water flow and sometimes encounters oil droplets, while, probe B still keeps at low voltage, which indicates that the local flow pattern is still in continuous

water flow without any oil droplets. According to the analysis of all probe signals, we can see that water-in-oil flow pattern is predominant in the upper side of the pipe, oil-in-water pattern often takes place in the bottom side of the pipe, and at the whole pipe section, the flow behavior presents complex TF flow pattern.

The D W/O flow pattern occurs at high oil superficial velocities and low to moderate water superficial velocities. In this flow pattern, oil presents as continuous phase in whole pipe section, while water is dispersed phase. The transition to D W/O originates with the increasing of oil flow rate in TF flow pattern. Fig. 7d shows typical probe signals in D W/O flow pattern. All the five probes signals show the characters of water-in-oil flow patterns. There are more dispersed water droplets at lower side of the pipe, while in the top side of the pipe, such as location of probe A and C, there are almost pure oil phase flow without water droplets. From the analysis of probe signals, it can be seen that the mini-conductance probes are sensitive to local flow pattern transition and can be used to identify different inclined oil–water flow patterns.

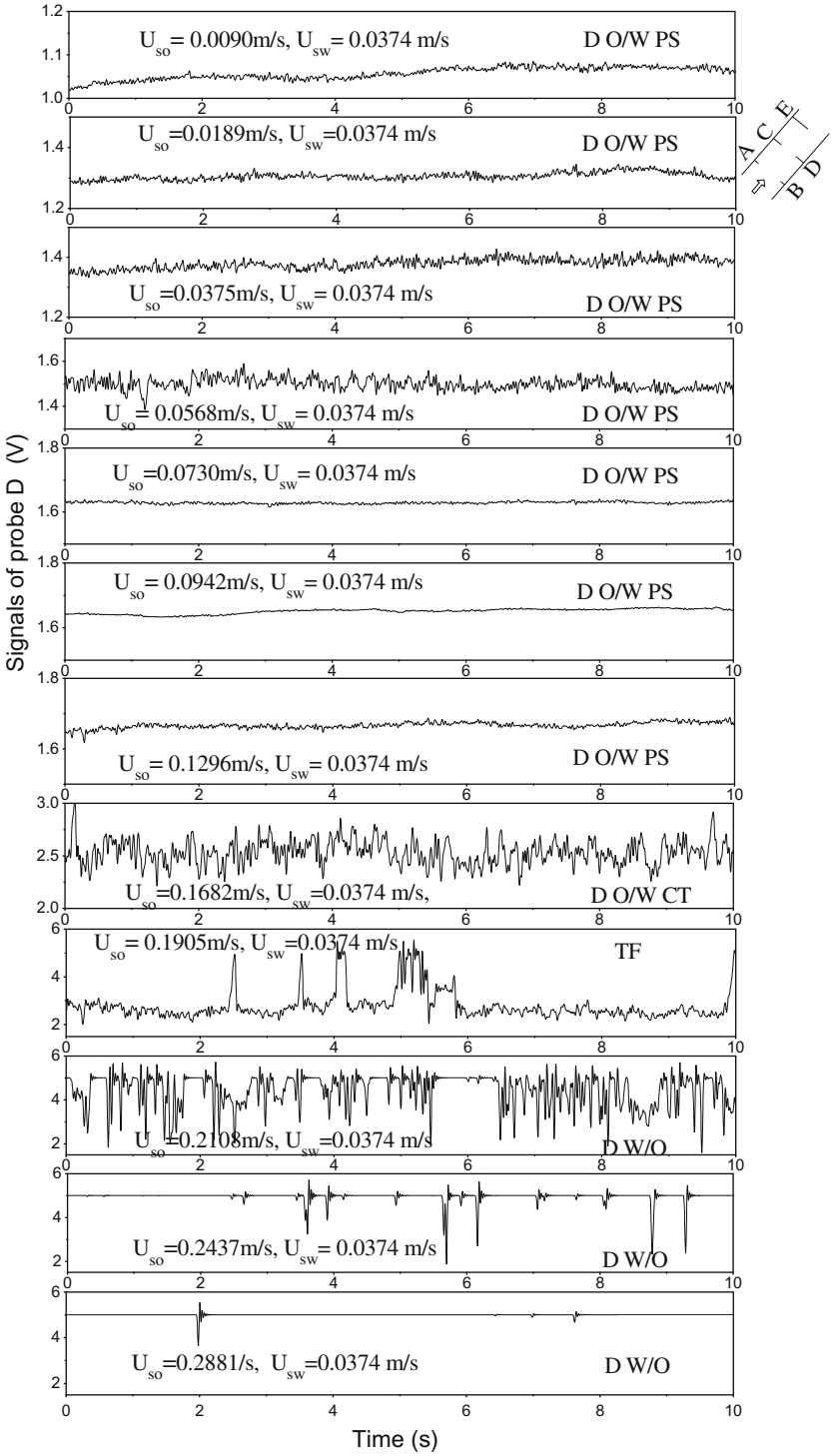

(d) probe D

Fig. 8 (*continued*)

Fig. 8 shows the mini-conductance probe signals when the oil superficial velocity increases from 0.0090 to 0.2881 m/s with the water superficial velocity fixed at 0.3047 m/s. The signal level of each mini-conductance probes, as shown in Fig. 8, reflects the flow pattern evolution trend from D O/W PS to D O/W CT, DO/W CT to TF, and TF to D W/O. With combinations of the mini-conductance probes and high speed VCR, we can make reasonable and dependable flow pattern definition in our experiment.

3.2. VMEA conductance probe signals

The signals measured from VMEA probe mainly reflect global conductance character of inclined oil–water mixed fluids. Fig. 9 shows the VMEA probe signals at different oil superficial velocities when U_{sw} is fixed at 0.0374 m/s at 45°. Obviously, the signals in Fig. 9 can be classified into three regions, region-I is greater than 2 V, region-II is less than 2 V and greater than 1 V, and region-III is less than 1 V. Comparing with mini-conductance probe signals,

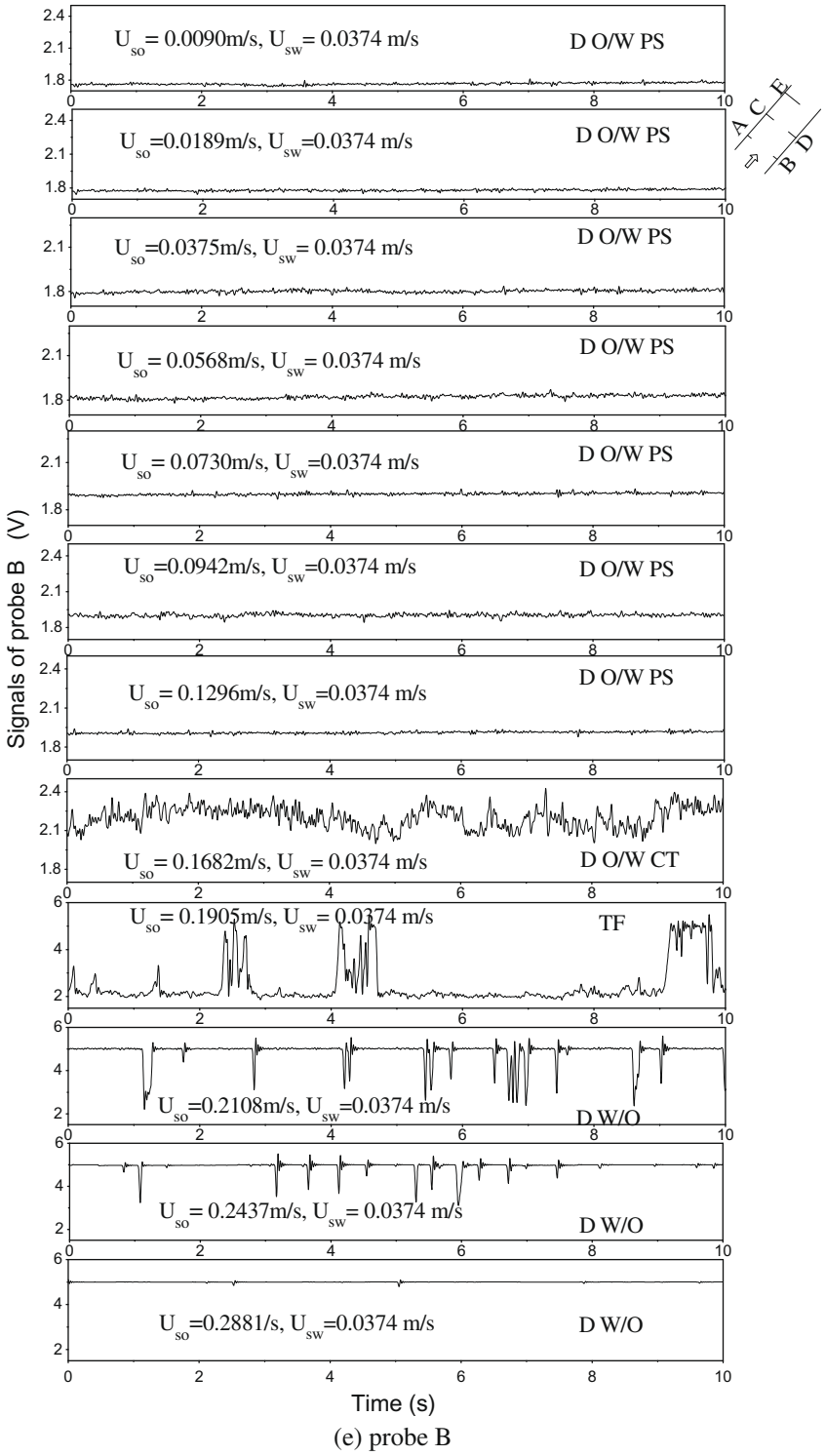

Fig. 8 (*continued*)

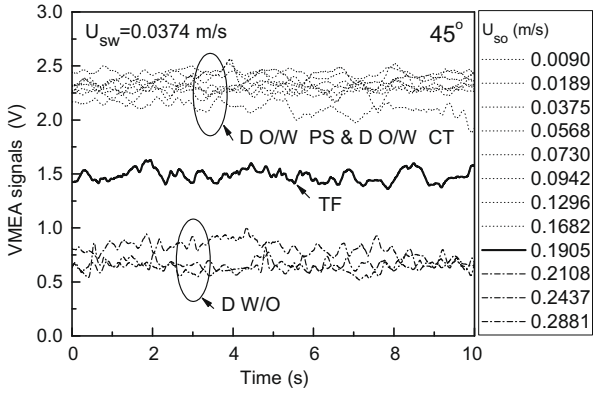

Fig. 9. VMEA signals changing with the increasing of oil phase flow rate at fixed water phase flow rate (inclination 45°, U_{sw} = 0.0374 m/s, U_{so} = 0.0090–0.2881 m/s).

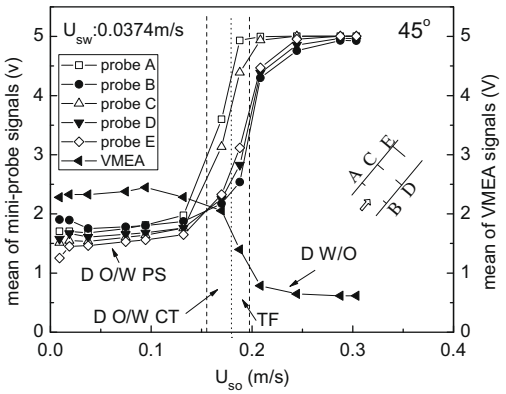

Fig. 11. Comparative schematics of mean of VMEA probe signals and that of mini-conductance probe signals with the increasing of oil phase flow rate at fixed water phase flow rate (inclination 45°, U_{sw} = 0.0374 m/s).

the three regions are consistent with three flow patterns: region-I corresponds to water-dominated flow pattern, including D O/W PS and D O/W CT flow pattern, region-II corresponds to TF flow pattern, and region-III corresponds to D W/O flow pattern.

Fig. 10 shows the mean of VMEA probe signals in all flow conditions. That is, U_{so} and U_{sw} are in the range of 0.0052–0.3306 m/s, and inclination angles are 15° and 45° from vertical, respectively. When U_{sw} is lower than 0.0929 m/s, VMEA probe signals will decrease with the increasing of oil flow rate, when U_{sw} is greater than 0.1321 m/s, VMEA probe signals are always higher than 2 V at any oil flow rate. This indicates that the corresponding flow pattern is water-dominated flow. The decrease of signal amplitude not only reflects the decreasing of water volume fraction in the pipe, but also indicates the fact that the flow pattern is evolving from D O/W PS to D W/O flow pattern. From the VMEA probe signals distribution, as shown in Fig. 10, we can find that there also exist three regions that are consistent with the description of Fig. 9. Region-I, greater than 2 V, reflects the character of oil-in-water flow pattern, where water is continuous phase. Region-III, lower than 1 V, reflects the character of water-in-oil flow pattern, where oil is continuous phase. The internal region-II reflects the flow pattern transition from water-dominated to oil-dominated pattern, and the significant decrease of signal amplitude in this region reflects the characters of unsteady TF flow pattern. Although the mean of VMEA probe signals can well reflect TF flow pattern, it is difficult to distinguish between D O/W PS and D O/W CT directly. Since the mini-conductance probes are sensitive to flow pattern transition, it is necessary to combine mini-conductance probes with VMEA probe to completely analyze the flow patterns under different flow conditions.

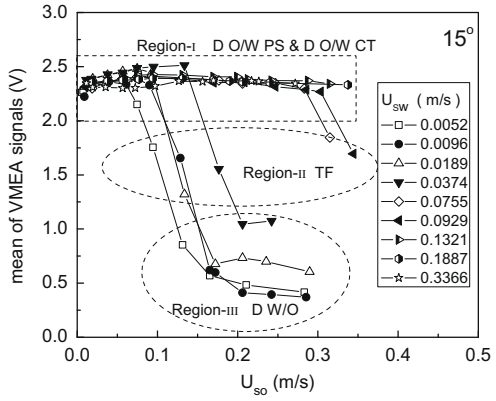

(a) Inclination 15°

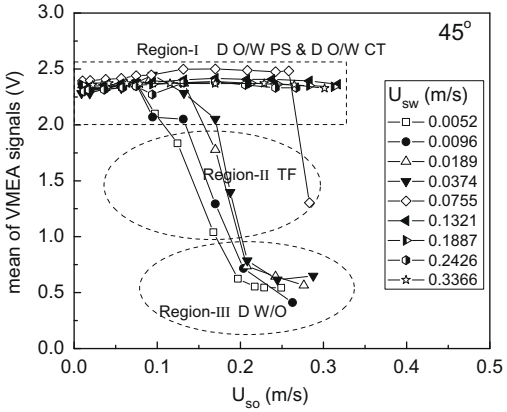

(b) Inclination 45°

Fig. 10. Mean of VMEA probe signals in all flow conditions.

Fig. 11 shows the mean of mini-conductance probe signals and that of VMEA probe with the increasing of U_{so} when U_{sw} is fixed at 0.0374 m/s at 45°. Since high voltage level in mini-conductance probe signals represents oil phase and low voltage level represents water phase, in water-dominated flow patterns, the mean value of mini probe signals will increase with the increasing of oil flow rate, while the trend of VMEA probe signals is on the contrary comparing with mini-conductance probe signals during the flow pattern evolution.

3.3. Inclined oil–water flow pattern map

The combination analysis of mini-conductance probe signals (see Section 3.1), VMEA probe signals (see Section 3.2) and video recordings can ensure the exact identification of inclined oil–water flow patterns. Fig. 12 shows the inclined oil–water flow pattern maps in 125 mm ID pipe at 15° and 45° from vertical, respectively.

The D O/W PS pattern is predominated for both U_{so} and U_{sw} in the range of 0.0052–0.3306 m/s, while the regions of D O/W CT and TF flow pattern are quite narrow in these experimental flow conditions, which is different with the conclusions of Flores in smaller diameter pipe. The flow pattern transitional boundaries are also different with Flores et al. (1999).

4. Nonlinear dynamic characteristics of inclined oil–water flow patterns

In early studies, it has been proved that nonlinear time series analysis method is an effective tool for understanding the flow

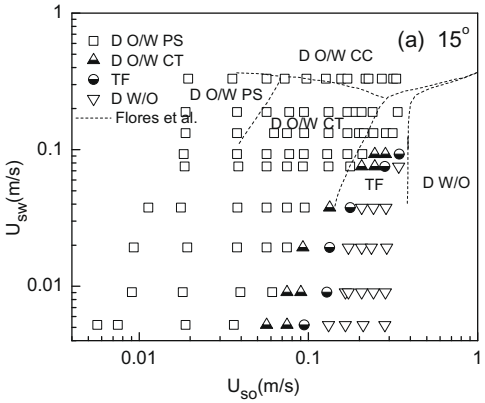

(a) Inclination 15°

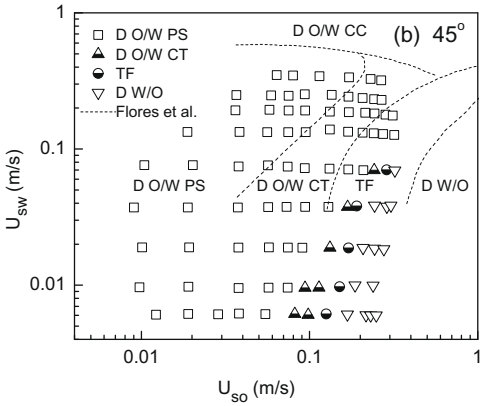

(b) Inclination 45°

Fig. 12. Inclined oil–water two phase flow pattern maps in 125 mm inner diameter pipe.

dynamic characteristics from multiphase flow signals (Franca et al., 1991; Oddie, 1991; Rawes et al., 1994; Yeung et al., 1994; Johnsson et al., 2000; Wu et al., 2001; Jin et al., 2003; Jana et al., 2006; Lee et al., 2008; Gao and Jin, 2009). Recurrence plot and recurrence qualification analysis (Eckmann et al., 1987; Zbilut and Webber, 1992) have proved themselves particularly suitable and flexible analysis tool for many complex systems in recent years. Our group first applies this analysis method to vertical and deviated oil–water flow pattern identification (Jin et al., 2006; Zong and Jin, 2008). Recently, Gandhi et al. (2008) predicted local gas holdup for bubble column reactor by using chaotic measure quantities of recurrence quantification analysis in soft-measurement model. In this study, we propose a new combination analysis method of recurrence quantification analysis for inclined oil–water flows.

4.1. Recurrence plot and recurrence qualification analysis

The embedding theory introduced by Takens (1981) is the base of phase space reconstruction; Abarbanel et al. (1993) summarized the analysis methods of observed chaotic data in physical systems. For VMEA probe time series $s(it)$, $i = 1, 2, \ldots, n$, (t is time interval, n is total number of the time series), choosing τ delay time and N embedding dimension, the points $\mathbf{X}(k)$ in phase space is

$$\begin{aligned}\mathbf{X}(k) &= \{s_1(k), s_2(k), \cdots, s_N(k)\} \\ &= \{s(kt), s(kt+\tau), \cdots, s[kt+(N-1)\tau]\}\end{aligned} \quad (1)$$

where $k = 1, 2, \ldots, M$, $M = n - (N-1) * \tau/t$ is total number of points in phase space.

Recurrence plot (RP) describes the dynamic behavior of trajectory $\mathbf{X}_i \in \mathbf{R}^N$ with the change of delay time, which denotes the recurrence state of trajectories in phase space. The representation is based on matrix

$$R_{i,j} = \Theta(\varepsilon - \|\mathbf{X}_i - \mathbf{X}_j\|), \quad i,j = 1, \ldots, M \quad (2)$$

where M is total points of trajectory $\boldsymbol{X}_i$, $\varepsilon = \alpha \cdot std(s(it))$ is a predefined distance threshold, $std(s(it))$ is the standard deviation of observed data, and α is a predefined threshold. $\|\cdot\|$ is Euclidean norm, $\Theta(\cdot)$ is Heaviside function. The matrix consists of the values 1 and 0 only. The graphical representation is $M \times M$ grid of points, which are encoded as black for 1 and white for 0. A black point in RP means that the system falls into a ε-neighborhood of the corresponding point in phase space.

To quantify the structures of RP, Zbilut and Webber (1992) proposed recurrence quantification analysis (RQA) method.

Recurrence Rate (*RR*) is a measure of density of recurrence points in RP, which is defined as the ratio between the number of all recurrence points and total number of points in RP.

$$RR = \frac{1}{N^2}\sum_{i,j=1}^{N} R_{i,j} \quad (3)$$

Determinism (*DET*) is the ratio of recurrence points forming diagonal structures to all recurrence points.

$$DET = \frac{\sum_{l=l_{\min}}^{N-1} l \cdot P(l)}{\sum_{i,j=1}^{N} R_{i,j}} \quad (4)$$

where $l_{\min} = 2$, $P(l)$ denotes the probability to find a diagonal line of length l in RP. *DET* can distinguish the recurrence points forming line segments with discrete recurrence points.

Average Diagonal Line Length (*L*) is the average time that two segments of the trajectory are close to each other and can be interpreted as the mean prediction time.

$$L = \frac{\sum_{l=l_{\min}}^{N-1} l \cdot P(l)}{\sum_{l=l_{\min}}^{N-1} P(l)} \quad (5)$$

Analogous to the definition of *DET* and *L*, Marwan et al. (2002) proposed two new measures of complexity, which are *Laminarity* (*LAM*) and *Trapping Time* (*TT*) respectively. *Laminarity* (*LAM*) is the ratio between the recurrence points forming vertical structures and the entire set of recurrence points.

$$LAM = \frac{\sum_{v=v_{\min}}^{N} v \cdot P(v)}{\sum_{v=1}^{N} v \cdot P(v)} \quad (6)$$

where $v_{\min} = 2$, $P(v)$ denotes the probability of vertical line of length v in RP. *LAM* is a measure of the amount of vertical structures in the whole RP and represents the occurrence of laminar states in the system without, however, describing the length of these laminar phases. *LAM* will decrease if the RP consists of more single recurrence points than vertical structures.

Analogous to the definition of *Average Diagonal Line Length*, *Trapping Time* (*TT*) is the average length of vertical structures in RP

$$TT = \frac{\sum_{v=2}^{N} v \cdot P(v)}{\sum_{v=2}^{N} P(v)} \quad (7)$$

TT contains information about the amount and the length of the vertical structures in RP. It measures the mean time that the system will abide at a specific state or how long the state will be trapped.

Fig. 13 shows the RP of the VMEA probe signals in different flow patterns for different oil superficial velocities when U_{sw} = 0.0374 m/s at inclined 45°. As can be seen, when U_{so} ranging from 0.0090 m/s to 0.1296 m/s, block intermittent texture can be clearly detected from the RP corresponding to D O/W PS flow pattern.

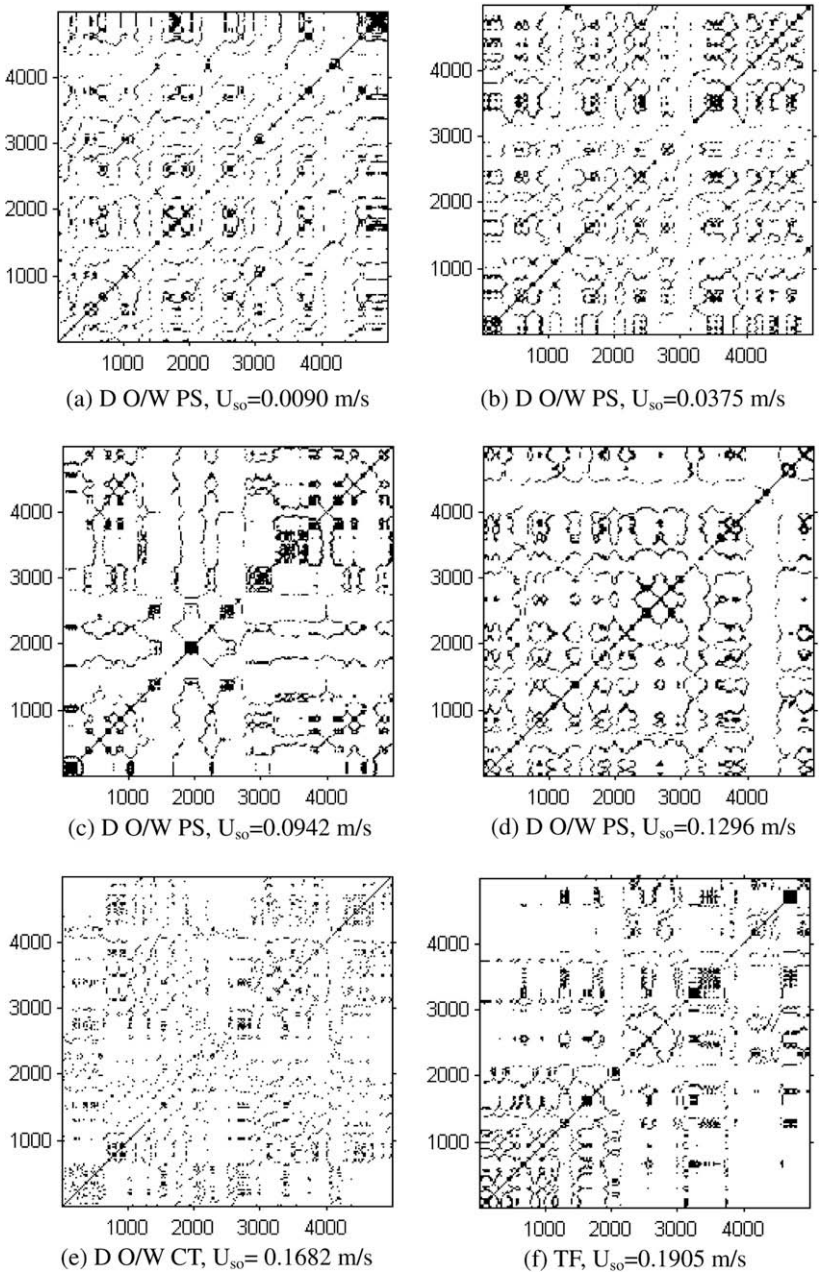

Fig. 13. Recurrence plot of VMEA probe signals in different flow patterns (inclination 45°, U_{sw} = 0.0374 m/s, U_{so} = 0.0090–0.2881 m/s, N = 3, τ = 3, $\varepsilon = 0.25 \cdot std(s(it))$).

When U_{so} = 0.1682 m/s, for the RP corresponding to D O/W CT flow pattern, there are much less structures and the lines are no matter in diagonal or vertical direction. When U_{so} increases to 0.1905 m/s, both the line structures and block textures in the RP of TF pattern become higher than that of D O/W CT flow pattern, and some drift structures can be detected. From the above analysis, we can find that the line structures in RP will change with flow pattern transition, which can be validated by RQA quantities more clearly in the following part.

Figs. 14 and 15 show the results of RQA on VMEA probe signals in D O/W PS, D O/W CT and TF flow pattern. Though the results of D O/W PS and TF flow pattern are mixed with each other, the results of D O/W CT flow pattern are markedly different with other two flow patterns. Taking *RR* for example, in D O/W PS flow pattern, *RR* locate in the range of 0.06–0.12 with the increasing of oil flow rates, then it will decrease to lower than 0.06 in D O/W CT flow pattern and finally increase to higher than 0.06 in TF flow pattern. As can be seen, the *RR* of D O/W PS flow pattern is higher than that of D O/W CT flow pattern. In fact, there is better intermittent motion of the pseudoslug flow structure in D O/W PS flow pattern, while the pseudoslug flow structure will disappear in D O/W CT flow pattern, which may cause the decrease of recurrence property and the differences of *RR* for D O/WPS and D O/W CT flow pattern. Other results of RQA are consistent with *RR* also.

Though the RQA results of D O/W PS and TF flow pattern are mixed with each other, these two flow patterns can be differentiated easily by the mean of VMEA signals just as shown in Section 3.2. It is enough for RQA to distinguish between D O/W PS and D O/W CT flow pattern. Since the definitions of *LAM* and *TT* are very similar to that of *DET* and *L*, the flow pattern distribution of D O/W PS and D O/W CT can be seen from either Fig. 16 (*LAM*–*DET* plane) or Fig. 17 (*TT*–*L* plane). Hence, we can clearly identify D O/W PS and D O/W CT flow pattern with the help of RQA quantities.

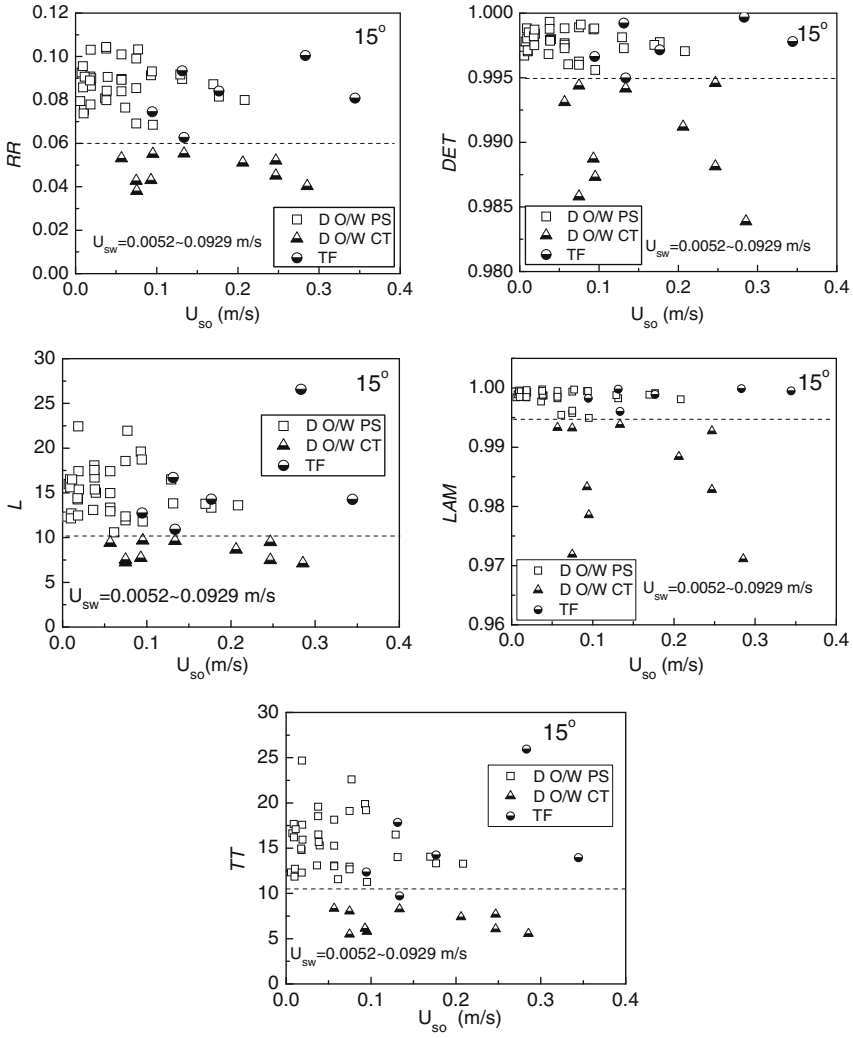

Fig. 14. Relationship between recurrence quantification analysis results and flow patterns in all flow conditions (inclination 15°).

4.2. Attractor geometry morphological characteristics

Annunziato and Abarbanel (1999) and Annunziato et al. (1999) proposed attractor morphologic description method, and applied in flame detection and flow pattern classification. The research showed that this method could rapidly get good results in flow pattern classification. Llauró and Llop (2006) analyzed the flow patterns of gas–solid flows in fluidized beds by using this method and got good classification results. Xiao and Jin (2007) optimized the choice of reference sections, applied it in pressure fluctuation signals of gas–liquid two phase flow in vertical upward pipe, and realized effective flow pattern classification. Zheng et al. (2008) differentiated bubble flow and slug flow pattern of gas–liquid flows in nontransparent stainless steel pipe by this method, and found that the slope of attractor moments $M_{1,2}$ and $M_{2,2}$ are a pair of effective parameters to identify flow patterns. In fact, only the characteristics of attractor moments changing with delay time are extracted in above literatures. In this study, new measures describing attractor characteristics are defined, such as attractor area, attractor long axis and short axis, the change of above measures with delay time are studied. The combination of above measures is expected to identify inclined oil–water flow patterns.

In two-dimensional phase space, the trajectory points will be $\mathbf{X}_i = (x_i, y_i)$, where $x_i = s(it)$ and $y_i = s(it + \tau)$, $s(it)$ is the observed time series, t is sampling interval and τ is delay time. To extract the attractor characteristics proposed by Annunziato and Abarbanel (1999) and Annunziato et al. (1999), the bisector of first and third quadrants is selected as principal axis; the bisector of second and fourth quadrants is selected as secondary axis. The distances of each point to the two axes and original point are defined as

$$d_{1,i} = \frac{\sqrt{2}}{2}(x_i - y_i) \tag{8}$$

$$d_{2,i} = \frac{\sqrt{2}}{2}(x_i + y_i) \tag{9}$$

$$d_{3,i} = \sqrt{x_i^2 + y_i^2} \tag{10}$$

j (j = 1, 2, 3, 4) order attractor moments for each distance are also defined as

$$M_{m,j}(\tau) = \frac{\sum_{i=1}^{M} d_{m,i}^{j}}{M} \tag{11}$$

where M is total number of points in attractor and m = 1, 2, 3 denotes the kind of distance.

Attractor area $A(\tau)$ is defined as the area surrounded by the outline of the attractor trajectory in two-dimensional phase space, which is computed by cumulative integration in the following three steps.

The first step is rotation and non-overlap division in x-axis. The attractor will be rotated 45° to let the principal axis in x-axis

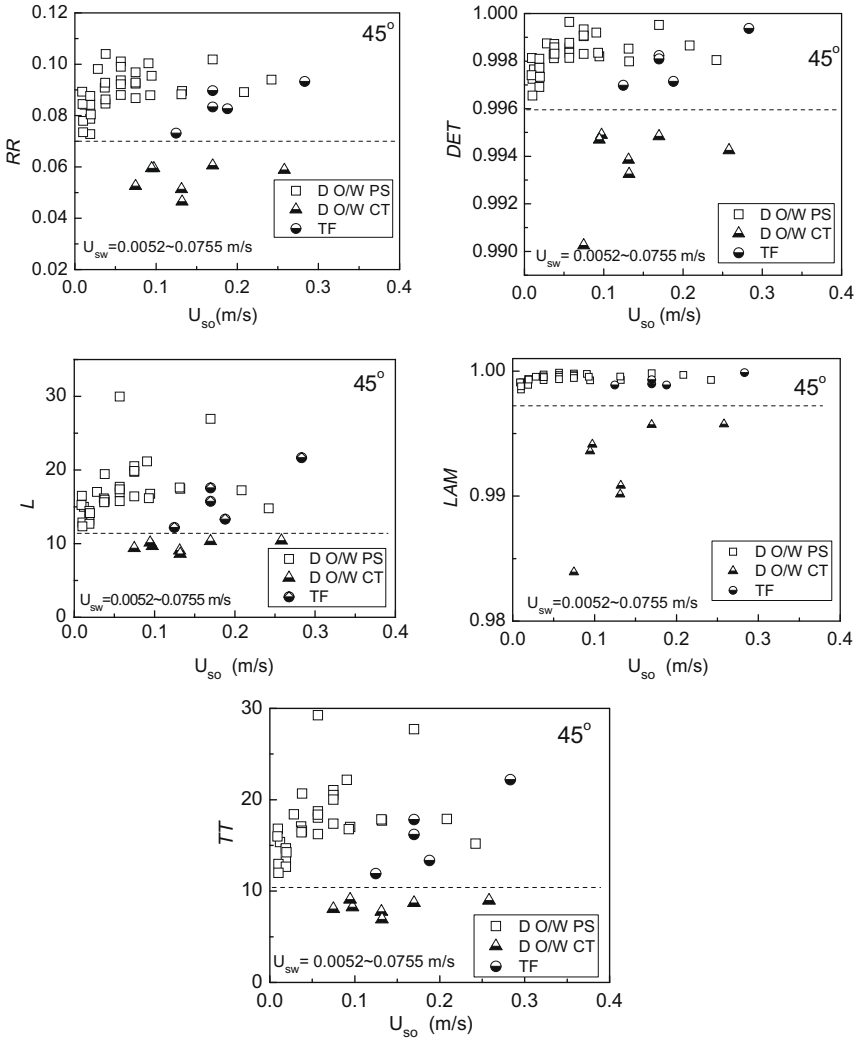

Fig. 15. Relationship between recurrence quantification analysis results and flow patterns in all flow conditions (inclination 45°).

direction and the secondary axis in *y-axis* direction for the convenience of computation, then, the maximal difference in *x*-axis direction is computed by

$$\Delta x = \max(x_i) - \min(x_i), \quad i \in 1, \ldots, N \tag{12}$$

The maximal distance Δx is equally divided into K intervals, with each interval length $l = \Delta x/K$.

The second step is searching maximal difference in *y*-axis. The point $\mathbf{X}_i$ meets

$$\min(x_i) + l \cdot (j-1) \leqslant x_k < \min(x_i) + l \cdot j, \quad k \in 1, \ldots, N, \ j \in 1, \ldots, K \tag{13}$$

The maximal difference in *y*-axis direction in each interval is

$$\Delta y_k = \max(y_k) - \min(y_k) \tag{14}$$

Then, the attractor area $A(\tau)$ is integrated by

$$A(\tau) = \lim_{K \to \infty} \sum_{k=1}^{k=K} \Delta y_k \cdot \frac{\Delta x}{K} \tag{15}$$

where K is selected 500.

The attractor long axis $L_{\text{axis}}(\tau)$ is defined as the maximal distance between two points in principal axis

$$L_{\text{axis}}(\tau) = \max(\mathbf{X}_i - \mathbf{Y}_i) \tag{16}$$

where $\mathbf{X}_i$ and $\mathbf{Y}_i$ are trajectory points in principal axis.

The attractor short axis $S_{\text{axis}}(\tau)$ is defined as the maximal distance between two points in secondary axis

$$S_{\text{axis}}(\tau) = \max(\mathbf{X}_i - \mathbf{Y}_i) \tag{17}$$

where $\mathbf{X}_i$ and $\mathbf{Y}_i$ are trajectory points in secondary axis.

In this study, the characteristics of attractor moments and area are extracted here based on the VMEA probe signals. Moreover, the $L_{\text{axis}}(\tau)$ and $S_{\text{axis}}(\tau)$ are not suitable for extracting the attractor characteristics.

4.3. The extracting of attractor geometry morphological characteristics

Figs. 18 and 19 show the dynamic attractor shape changing with delay time in D O/W PS and D O/W CT flow pattern respectively, which reflects the process of dynamic attractor from compressed line to completely unfolded states. With the definition of attractor moments and area, the curve of $M_{m,j}(\tau) \sim \tau$ and $A(\tau) \sim \tau$ can be figured out, such as the curve $M_{1,2}(\tau) \sim \tau$ and $A(\tau) \sim \tau$ in Fig. 20.

If the curves $M_{m,j}(\tau) \sim \tau$ or $A(\tau) \sim \tau$ appears maximum or minimum after certain delay time, which is defined as transform delay time τ_f. If there is no extreme, the delay time corresponding sudden change of slope can also be defined as the transform delay time. The part before τ_f is called first zone, and second zone after τ_f.

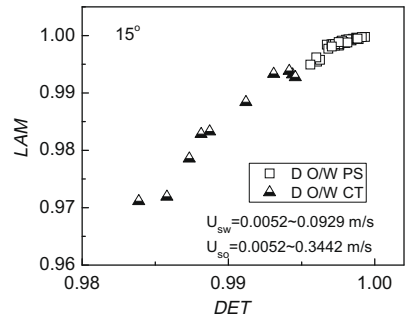

(a) Inclination 15°

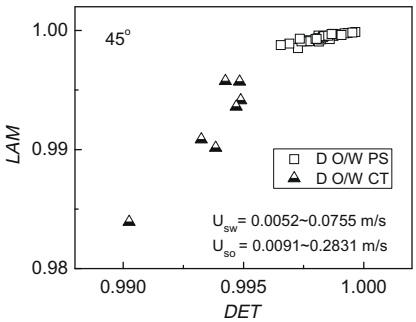

(b) Inclination 45°

Fig. 16. D O/W PS and D O/W CT flow pattern distribution in *LAM–DET* plane.

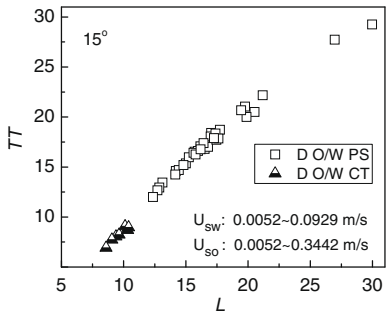

(a) Inclination 15°

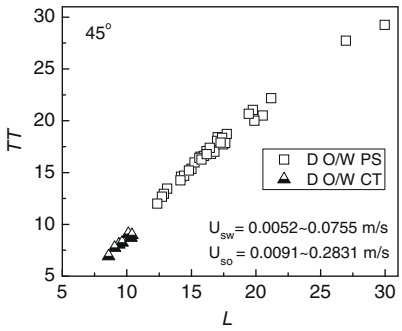

(b) Inclination 45°

Fig. 17. D O/W PS and D O/W CT flow pattern distribution in *TT–L* plane.

The first zone corresponds to attractor unfolding process from compressed to unfolding state at suitable delay time, this zone is approximately linear process, so the slope of the curves can serve as characteristics of attractor, namely the attractor geometry morphological characteristics, denoted as $SM_{m,j}$ and SA respectively, which means the growth rate of the attractor moments and area. The following equation should be satisfied.

$$M_{m,j}(\tau) \approx SM_{m,j} \cdot \tau + M_{m,j}(0) \quad (0 \leqslant \tau \leqslant \tau_f) \tag{18}$$

$$A(\tau) \approx SA \cdot \tau + A(0) \quad (0 \leqslant \tau \leqslant \tau_f) \tag{19}$$

where $M_{m,j}(0)$ and $S(0)$ are intercept of each curve. As the slope of moments or area in first zone are taken as attractor geometry morphological characteristics, which is not affected by traditional method of choosing delay time. The second zone corresponds to completely unfolded state of the attractor structure.

Fig. 20 shows the curves of the moments $M_{1,2}(\tau)$ and area $A(\tau)$ with the change of delay time τ in water-dominated flow pattern when U_{sw} = 0.0374 m/s with different U_{so} at 45°. Fig. 20a shows

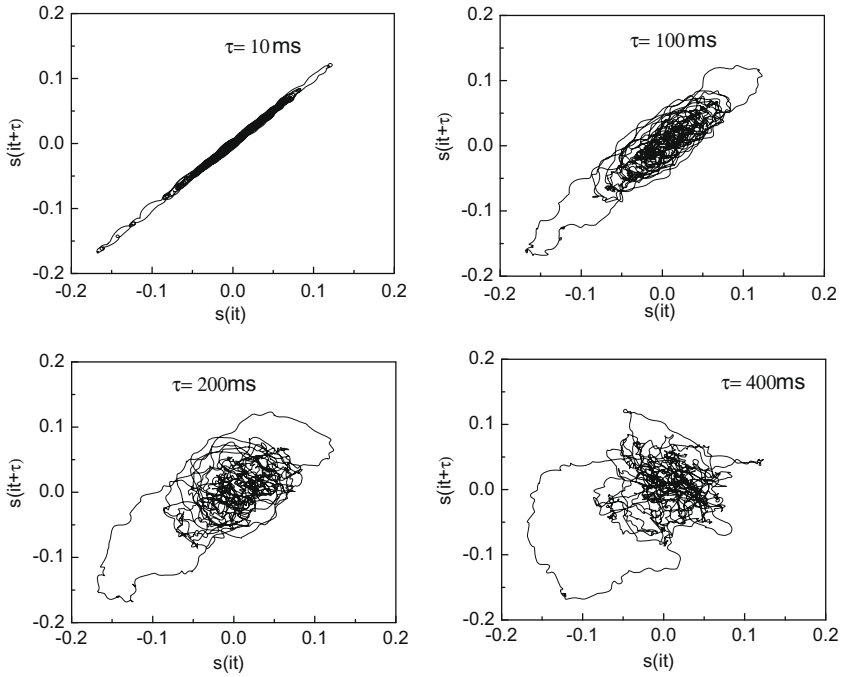

Fig. 18. Dynamic attractor changing with the increasing of delay time (inclination 45°, U_{sw} = 0.0374 m/s, U_{so} = 0.0730 m/s, D O/W PS flow pattern).

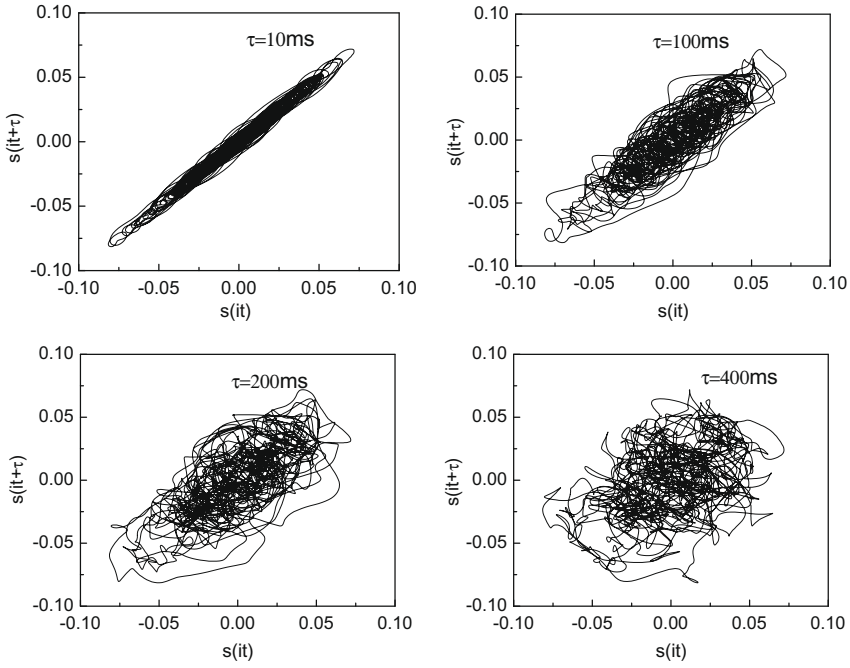

Fig. 19. Dynamic attractor changing with the increasing of delay time (inclination 45°, U_{sw} = 0.0374 m/s, U_{so} = 0.1682 m/s, D O/W CT flow pattern).

the curve $M_{1,2}(\tau) \sim \tau$, the slope of moment $M_{1,2}$ in the first zone are markedly different for D O/W PS and D O/W CT flow pattern, and the flow pattern distribution in $SM_{1,2}$–$SM_{2,2}$ plane are shown in Fig. 21. The absolute value of slope of the attractor moments in D O/W PS are generally higher than that of D O/W CT flow pattern, which indicates that the unfolding process of attractor in D O/W PS is faster than that of D O/W CT flow pattern.

Fig. 20b shows the change of attractor area $A(\tau)$ with the increase of delay time τ, which indicates that the slope of area SA in the first zone and the terminal area $\overline{A}$ of D O/W PS flow are both higher than that of D O/W CT flow pattern. The flow pattern distribution of D O/W PS and D O/W CT flow pattern in $SA - \overline{A}$ plane is shown in Fig. 22, from which the good flow pattern classification results can be seen.

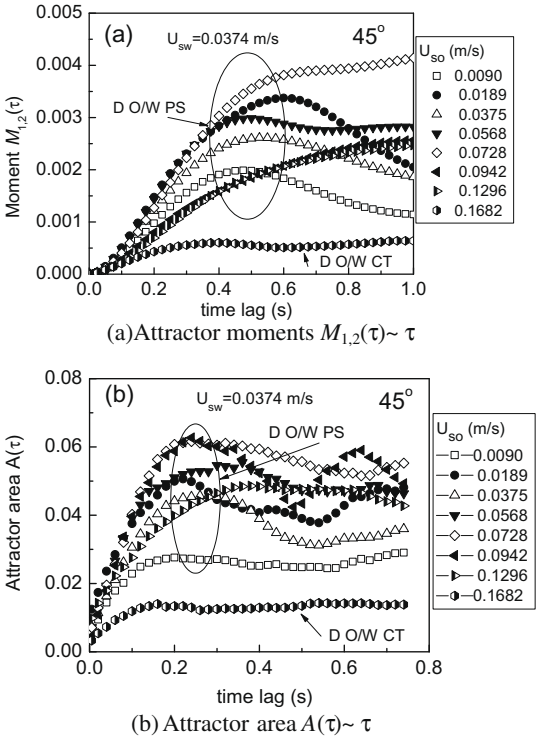

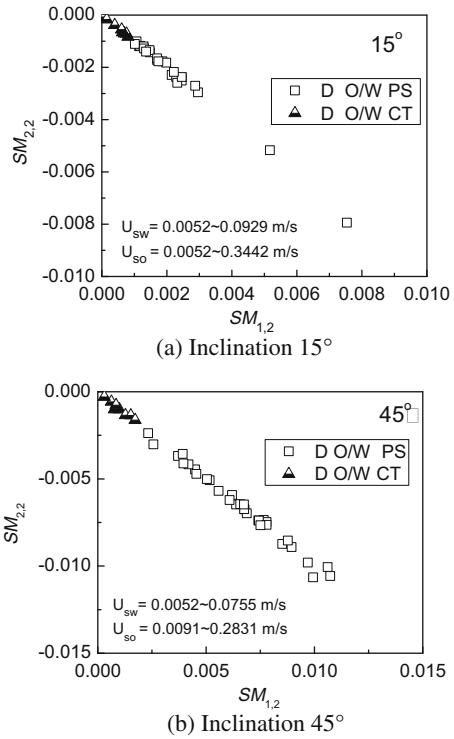

Fig. 20. Curves of attractor moment $M_{1,2}(\tau)$ and area $A(\tau)$ changing with delay time τ.

Fig. 21. D O/W PS and D O/W CT flow pattern distribution in $SM_{1,2}$–$SM_{2,2}$ plane.

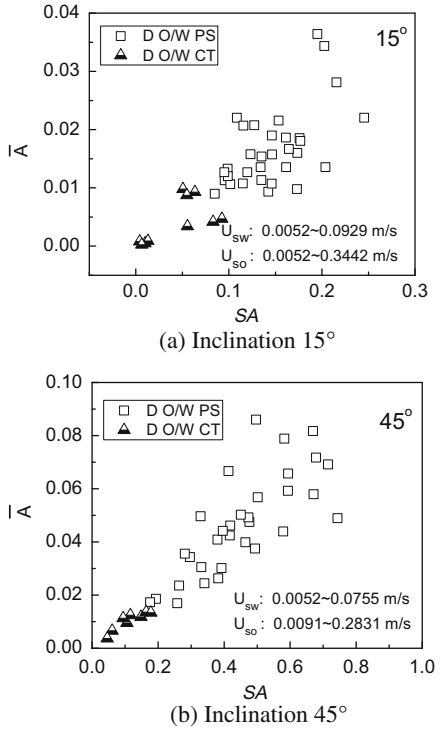

Fig. 22. D O/W PS and D O/W CT flow pattern distribution in $SA - \overline{A}$ plane.

5. Conclusions

In summary, we have experimentally investigated the flow structures of inclined oil–water two phase flow in large diameter pipe by the combined application of VMEA and mini-conductance probes. Though DO/W PS and D O/W CT flow pattern cannot be directly identified by simple statistics of VMEA probe signals, they can be effectively distinguished with each other by nonlinear analysis method. Through analyzing the mini-conductance probe signals, we not only exactly identify the four inclined oil–water two phase flow patterns but also provide the corresponding flow pattern maps. Moreover, it should be pointed out that, since the pipe diameter in this experiment is markedly different from that of Flores, D O/W PS flow pattern is predominant, while D O/W CT and TF flow pattern only exist in a quite narrow region in flow pattern maps, and the flow pattern transition boundaries are also different from that in Flores flow pattern maps.

Using recurrence quantification analysis and attractor geometry morphological description method, we have analyzed the signal time series measured from VEMA sensor and achieved good flow pattern classification results. Our research indicates that the nonlinear dynamic analysis methods can be effectively applied to quantitatively characterize the inclined oil–water two phase flow pattern transitions.

Acknowledgements

Project supported by the National Natural Science Foundation of China (Grant Nos. 50674070, 60374041) and the National High Technology Research and Development Program of China (Grant No. 2007AA06Z231).

References

Abarbanel, H.D.I., Brown, R., Sidorowich, J.J., Tsimring, L.S., 1993. The analysis of observed chaotic data in physical systems. Rev. Mod. Phys. 65, 1331–1392.

Al-Wahaibi, T., Angeli, P., 2007. Transition between stratified and non-stratified horizontal oil–water flow. Part I: stability analysis. Chem. Eng. Sci. 62, 2915–2928.

Al-Wahaibi, T., Smith, M., Angeli, P., 2007. Transition between stratified and non-stratified horizontal oil–water flow. Part II: mechanism of drop formation. Chem. Eng. Sci. 62, 2929–2940.

Angeli, P., Hewitt, G.F., 2000. Flow structure in horizontal oil–water flow. Int. J. Multiphase Flow 26, 1117–1140.

Annunziato, M., Abarbanel, H.D.I., 1999. Non linear dynamics for classification of multiphase flow regimes. In: Proceedings of International Conference on Soft Computing, Genova, Italy.

Annunziato, M., Bertini, I., Piacentini, M., Pannicelli, A., 1999. Flame dynamics charaterisation by chaotic analysis of image sequences. In: 36 International Heat Transfer and Fluid Mechanics Institute. Sacramento, USA, pp. 13–30 (Characterisation).

Brauner, N., 2002. Liquid–liquid two phase flow systems. In: Bertola, V. (Ed.), Modeling and Control of Two Phase Flow Phenomena. CISM Center, Udine, Italy.

Davarzani, J., Sloan, L., Roesner, R.E., 1985. Research on simultaneous production logging instruments in multiphase flow loop. In: Paper SPE 14431, Presented at the 60th Annual Technical Conference and Exhibition of the Society of Petroleum Engineers Held in Las Vegas, 22–25 September.

Ding, Z.X., Ullah, K., Huang, Y., 1994. A comparison of predictive oil/water holdup models for production log interpretation in vertical and deviated wellbores. In: SPWLA 35th Annual Logging Symposium, Tulsa, 19–22 June.

Dong, F., Liu, X.P., Deng, X., Xu, L.J., Xu, L.A., 2001. Identification of two phase flow regimes in horizontal, inclined and vertical pipes. Meas. Sci. Technol. 12, 1069–1075.

Eckmann, J.P., Kamphorst, S.O., Ruelle, D., 1987. Recurrence plots of dynamical systems. Europhys. Lett. 5, 973–977.

Fairuzov, Y.V., Aernas-Medina, P., Verdejo-Fierro, J., Gonzalez-Islas, R., 2000. Flow pattern transitions in horizontal pipelines carrying oil–water mixtures: full-scale experiments. J. Energy Resour. Technol. 122, 169–176.

Flores, J.G., Chen, X.T., Sarica, C., Brill, J.P., 1999. Characterization of oil–water flow patterns in vertical and deviated wells. SPE Prod. Facil. 14, 102–109.

Franca, F., Acikgoz, M., Lahey, R.T., Clausse, A., 1991. The use of fractal techniques for flow regime identification. Int. J. Multiphase Flow 17, 545–552.

Gandhi, A.B., Joshi, J.B., Kulkarni, A.A., Jayaraman, V.K., Kulkarni, B.D., 2008. SVR-based prediction of point gas hold-up for bubble column reactor through recurrence quantification analysis of LDA time-series. Int. J. Multiphase Flow 34, 1099–1107.

Gao, Z.K., Jin, N.D., 2009. Flow-pattern identification and nonlinear dynamics of gas-liquid two phase flow in complex networks. Phys. Rev. E 79, 066303.

Hasan, A.R., Kabir, C.S., 1998. A simplified model for oil–water flow in vertical and deviated wellbores. In: Paper SPE 49163, SPE Annual Technical Conference and Exhibition, New Orleans, Louisiana, 27–30 September.

Hibiki, T., Situ, R., Mi, Y., Ishii, M., 2003. Local flow measurement of vertical upward bubbly flow in an annulus. Int. J. Heat Mass Transfer 46, 1479–1496.

Hill, A.D., Oolman, T., 1982. Production logging tool behavior in two phase inclined flow. J. Petrol. Technol. 34, 2432–2440.

Hogsett, S., Ishii, M., 1997. Local two phase flow measurements using sensor techniques. Nucl. Eng. Des. 175, 15–24.

Ishill, M., Kim, S., 2001. Micro four-sensor probe measurement of interfacial area transport for bubbly flow in round pipes. Nucl. Eng. Des. 205, 123–131.

Jana, A.K., Dasa, G., Das, P.K., 2006. Flow regime identification of two phase liquid–liquid upflow through vertical pipe. Chem. Eng. Sci. 61, 1500–1515.

Jin, N.D., Nie, X.B., Ren, Y.Y., Liu, X.B., 2003. Characterization of oil water two phase flow patterns based on nonlinear time series analysis. Flow Meas. Instrum. 14, 169–175.

Jin N.D., Zheng G.B., Dong F., Chen W.P., 2006. Application of chaotic recurrence plot analysis to identification of oil/water two phase flow patterns. In: Third International Conference on Fuzzy Systems and Knowledge Discovery, Xi'an, PR China, vol. 4223, pp. 1213–1216.

Jin, N.D., Zhao, X., Wang, J., Jia, X.H., Chen, W.P., 2008. Design and geometry optimization of a conductivity probe with a vertical multiple electrode array for measuring volume fraction and axial velocity of two phase flow. Meas. Sci. Technol. 19, 045403.

Johnsson, F., Zijerveld, R.C., Schouten, J.C., Van den Bleek, C.M., Leckner, B., 2000. Characterization of fluidization regimes by time-series analysis of pressure fluctuations. Int. J. Multiphase Flow 26, 663–715.

Lee, J.Y., Kim, N.S., Ishii, M., 2008. Flow regime identification using chaotic characteristics of two phase flow. Nucl. Eng. Des. 238, 945–957.

Llauró, F.X., Llop, M.F., 2006. Characterization and classification of fluidization regimes by non-linear analysis of pressure fluctuations. Int. J. Multiphase Flow 32, 1397–1404.

Lucas, G.P., 1995. Modelling velocity profiles in inclined multiphase flow to provide a priori information for flow imaging. Chem. Eng. J. 56, 167–173.

Lucas, G.P., Jin, N.D., 2001a. Investigation of a drift velocity model for predicting superficial velocities of oil and water in inclined oil-in-water pipe flows with a centre body. Meas. Sci. Technol. 12, 1546–1554.

Lucas, G.P., Jin, N.D., 2001b. Measurement of the homogeneous velocity of inclined oil-in-water flows using a resistance cross correlation flow meter. Meas. Sci. Technol. 12, 1529–1537.

Lucas, G.P., Mishra, R., 2005. Measurement of bubble velocity components in a swirling gas–liquid pipe flow using a local four-sensor conductance probe. Meas. Sci. Technol. 16, 749–758.

Lum, J.Y.L., Al-Wahaibi, T., Angeli, P., 2006. Upward and downward inclination oil–water flows. Int. J. Multiphase Flow 32, 413–435.

Marwan, N., Wessel, N., Meyerfeldt, U., Schirdewan, A., Kurths, J., 2002. Recurrence plot based measures of complexity and its application to heart rate variability data. Phys. Rev. E 66 (2), 26702.

Mobbs, S.D., Lucas, G.P., 1993. A turbulence model for inclined, bubbly flows. Appl. Sci. Res. 51, 263–268.

Mukherjee, H., Brill, J.P., Beggs, H.D., 1981. Experimental study of oil–water flow in inclined pipes. Trans. ASME 103, 56–66.

Oddie, G.M., 1991. On the detection of a low-dimensional attractor in disperse two-component (oil–water) flow in a vertical pipe. Flow Meas. Instrum. 2, 225–231.

Oddie, G., Shi, H., Durlofsky, L.J., Aziz, K., Pfeffer, B., Holmes, J.A., 2003. Experimental study of two and three phase flows in large diameter inclined pipes. Int. J. Multiphase Flow 29, 527–558.

Rawes, W., Oddie, G., Yeung, H.,1994. Estimating fractal dimension and number of degrees of freedom for multiphase flow regime identification. In: Proceedings of a Conference on ''Image Processing: Mathematical Methods and Applications" Oxford in September.

Tabeling, P., Pouliquen, O., Theron, B., Catala, G., 1991. Oil–water flows in deviated pipes: experimental study and modelling. In: Proceedings of the 5th International Conference on Multiphase Flow Production, Cannes, France, 19–21 June, pp. 294–306.

Takens, F., 1981. Dynamical System and Turbulence. Lecture Notes in Mathematics, vol. 898. Springer-Verlag, Berlin. pp. 366–381.

Trallero, J.L., Brill, J.P., 1996. A study of oil–water flow patterns in horizontal pipes. In: Paper SPE 36609, Presented at the SPE Annual Technical Conference and Exhibition Held in Denver, Colorado, USA, 6–9 October, pp. 363–375.

Vigneaux, P., Chenais, P., Hulin, J.P., 1988. Liquid–liquid flow in an inclined pipe. AIChE J. 34, 781–789.

Wu, Q., Ishii, M., 1999. Sensitivity study on double-sensor conductivity probe for the measurement of interfacial area concentration in bubbly flow. Int. J. Multiphase Flow 25, 155–173.

Wu, H.J., Zhou, F.D., Wu, Y.Y., 2001. Intelligent identification system of flow regime of oil–gas–water multiphase flow. Int. J. Multiphase Flow 27, 459–475.

Xiao, N., Jin, N.D., 2007. Research on flow pattern classification method of two phase flow based on chaotic attractor morphological characteristic. Acta Phys. Sin. 56 (9), 5149–5157.

Yeung, H., Oddie, G., Rawes, W.H.L., 1994. Characterisations of Air/Water Flows Using Chaotic Dynamical System Analysis. Flomeko 94 – Flow Measurement in the Mid'90s. 13–17 June, Glasgow.

Zavareh, F., Hill, A.D., Podio, A.L., 1988. Flow regimes in vertical and inclined oil/water flow in pipes. In: Paper SPE 18215, Presented at the 63rd Annual Technical Conference and Exhibition in Houston, Texas, 2–5 October, pp. 361–368.

Zbilut, J.P., Webber, Jr.C.L., 1992. Embeddings and delays as derived from quantification of recurrence plots. Phys. Lett. A 171, 199–203.

Zheng, G.B., Jin, N.D., Jia, X.H., Lv, P.J., Liu, X.B., 2008. Gas–liquid two phase flow measurement method based on combination instrument of turbine flowmeter and conductance sensor. Int. J. Multiphase Flow 34, 1031–1047.

Zong, Y.B., Jin, N.D., 2008. Multi-scale recurrence plot analysis of inclined oil–water two phase flow structure based on conductance fluctuation signals. Eur. Phys. J. Special Topics 164, 165–177.